Search

Proceedings of

2018 IEEE/CSAA Guidance, Navigation and Control Conference

IEEE/CSAA GNCC 2018

August 10-12, 2018
Xiamen, China

Sponsored by

Technical Sponsored by

Shi Xingwei	**0220**	SatB2.3
Shi Yan	**0499**	SatA11.61
Shi Yongxia	**0098**	SatB6.1
Shi Zhenqing	**0316**	SatA3.7
	0644	SatB3.6
Shu Leizheng	**0119**	SunB10.2
Shu Qibao	**0206**	SatB10.10
	0254	SatB10.30
Shu Xiangqian	**0427**	SunA12.20
Shuai-qi Zhu	**0038**	SunB10.1
Sinhmar Himani	**0618**	SunB5.4
Song Chuang	**0446**	SunA12.27
Song Dongliang	**0010**	SatA11.1
	0358	SatA5.7
Song Haitao	**0250**	SatB4.4
Song Hongyi	**0463**	SatA6.6
	0535	SatB1.5
Song Hua	**0524**	SunB5.1

An IMU/Sonar-based Extended Kalman Filter for Mini-UAV Localization in Indoor Environment

Xiangqian Shu, Lingyu Yang, Xiaoke Feng, Jing Zhang

Beihang Univ.

ABSTRACT

Micro Aerial Vehicles (MAV) have been seen rapid progress in the indoor entertaining, security monitoring, as well as search and rescue activities. The indoor localization with lightweight sensors in a Global Positioning System (GPS-denied) environment is a challenging topic for MAVs autonomous flight and path planning. This paper proposes a novel indoor localization approach relying on only the IMU and four ultrasonic sensors. Four mutually perpendicular installed ultrasonic sensors are used to provide distances of each direction. A prior map and an improved multiple rays model are constructed to approximate the measurement of the ultrasonic sensor. A fast algorithm to calculate the Jacobian matrix of the measurement function is given, then an Extended Kalman Filter (EKF) is conducted to fuse the information from IMU and the sonar sensor. The proposed algorithm is validated by the simulation and the results indicate good localization performance and robustness against compass measurement noise.

An IMU/Sonar-based Extended Kalman Filter for Mini-UAV Localization in Indoor Environment

Xiangqian Shu, Lingyu Yang, Xiaoke Feng, Jing Zhang

***Abstract*—Micro Aerial Vehicles (MAV) have been seen rapid progress in the indoor entertaining, security monitoring, as well as search and rescue activities. The indoor localization with lightweight sensors in a Global Positioning System (GPS-denied) environment is a challenging topic for MAVs autonomous flight and path planning. This paper proposes a novel indoor localization approach relying on only the IMU and four ultrasonic sensors. Four mutually perpendicular installed ultrasonic sensors are used to provide distances of each direction. A prior map and an improved multiple rays model are constructed to approximate the measurement of the ultrasonic sensor. A fast algorithm to calculate the Jacobian matrix of the measurement function is given, then an Extended Kalman Filter (EKF) is conducted to fuse the information from IMU and the sonar sensor. The proposed algorithm is validated by the simulation and the results indicate good localization performance and robustness against compass measurement noise.**

I. INTRODUCTION

The Micro Aerial Vehicle(MAV) has the characteristics of small size and high flying agility, it can replace human works in hazardous environment , adverse conditions and/or narrow space, and it has been widely applied to various fields[1][2][3]. One of the fundamental to flying the MAV autonomously is the ability of indoor localization. However, due to the strict restrictions on the size and weight, the available localization sensors for MAV are also limited. So how to utilize low-cost and lightweight sensor resources to locate the MAV in a complex and ever-changing indoor environment is a hot and challenging issue.

Most of the outdoor navigation algorithms are based on Global Positioning System(GPS), while the GPS signal is usually poor in the indoor environment. In order to achieve indoor localization, a variety of solutions are proposed[4], which are based on ranging sensors[5][6], Inertial Measurement Unit(IMU), cameras[7], WLAN[8], ZigBee[9] and radio frequency sensors[10]. In this paper, the above approaches are divided into two types by whether the localization sensors are placed on the UAV or not, i.e., the onboard-sensor-based approach and offboard-sensor-based approach.

The offboard-sensor-based approach needs to prearrange some equipment in the UAV's flight environment. Circket is an indoor localization system based on ultrasonic and radio frequency signals developed by the MIT[11], it consists of several beacons fixed on the ceiling and a moving signal receiver. The distance between the beacon and the receiver is calculated by the time difference of arrival(TDOA)，and the position of the receiver is estimated by the Kalman Filter(KF). In [12], multiple WiFi base stations are placed at known coordinates, the intensity of the WiFi signal is collected as the UAV traverses the base station and then converted into distance, and then different algorithms are used to estimate the location of UAV according to the number of signals collected. Another way of localization over WiFi is to use fingerprinting method. In [13], the fingerprint database is established by the WiFi signal intensity and a multi-core learning algorithm is used to estimate the UAV's position. In [14], the author combines the data from the IMU, Ultra Wide Band(UWB) and 3D laser scanner through the Kalman Filter to improve the accuracy of localization. In [15], an active base station system is proposed, a rotatable base station is used to reduce the signal measurement dead zone, thus the localization problem is considered as a nonlinear least squares problem. Newton's iterative method is used to calculate the optimal position and the localization accuracy depends on the number of base stations.

The offboard-sensor-based approach requires external device's assistance, thus it is hard to be applied to the unknown environment. As a result, many researchers have studied how to achieve localization through as few pre-installation devices as possible, most of these methods use vision or laser radar sensors. In [16], the data from IMU and lidars are used as input to the odometer, the position of the UAV and the map is given simultaneously. In [17], a landmarks-based method is introduced. Some simply shaped objects, such as walls, corners and edges, are chosen as landmarks. And 16 ultrasonic sensors are mounted around the mobile robot to identify and measure the distance to the landmarks. Then the robot's position can be given when two geometrical elements are successfully identified. In [18], the extracted and matched SIFT features are used to construct nonlinear least squares problems, then the pose of the UAV is solved by Gauss Newton method, which use IMU to estimate the initial value of the solution. In [19], the Harris corner detection algorithm is used to detect the corner points, and the corner points of the two adjacent images are matched to obtain an optimized objective function, then by the LM algorithm for nonlinear optimization, and finally get the UAVs pose. In [20], the lamp on the ceiling is used as landmark, through the extraction of feature points on the lamp and then real time localization can be realized by combining the relevant information of the landmark in the database. In [21], the lidar data is segmented using KD trees and then the PLICP algorithm is used to match the point sets of two adjacent scans, the error equation is constructed according to the distance between these matching points. through the iterative solution

Xiangqian Shu, Lingyu Yang, Xiaoke Feng and Jing Zhang are with the School of Automation Science and Electrical Engineering, Beihang University, Beijing, 100191 China. (Corresponding author: Lingyu Yang; Phone:8610-82316873, email: yanglingyu@buaa.edu.cn)

of the equation, the rotation and translation of two adjacent scans are calculated, and then the position of the robot is estimated. In [22], the author uses the planar object for positioning. First, the laser data is segmented and plane fitting. Then use a variant of the hill-climbing algorithm to match the planes in two adjacent scan data. Finally, 3 successful matching planes are selected to calculate the location of the robot based on the geometric relationship.

In summary, most of the offboard-sensor-based approach are based on distance sensor, usually place the base station on the ceiling, some use a large amount of ultrasonic to extract the geometric features of the environment. While most of the onboard-sensor-approach use vision sensors or lidar sensors, often have a large amount of computation due to the extraction and matching of feature and the nonlinear optimization step for position calculating. In contrast, we use only 4 ultrasonic sensors to achieve position estimation. The geometrical relations are used to deduce the Jacobian matrix of the observation equation. The computational complexity is low, which satisfies the limitation of MAV on computing resources.

This paper is organized as follows. The MAV platform and the ultrasonic measurement model are presented in Section II. The MAV system is modeled in the third section. Section IV presents the localization algorithm based on EKF. Section V validated the algorithm in the simulation environment and verifies the robustness of the algorithm.

II. THE MAV PLATFORM

The MAV used in this paper is in "X" configuration, and four ultrasonic rangefinders are installed along body axis for localization, as shown in Fig.1.

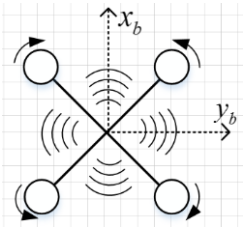

Figure 1. The MAV configuration and body reference frame

The airframe of the MAV and the ultrasonic sensors are shown in Fig.2, the weight of the MAV is about 75g and its wheelbase is 13.5 cm. The angular velocity and movement acceleration of MAV are measured by the MPU6000 IMU sensor, and the heading angle is provided by the magnetic sensor LSM303, and both have a sampling period of 8ms.The operating system runs on the flight control board is the PX4. It is easy to develop customized tasks, and all the data during the flight period are easy to store.

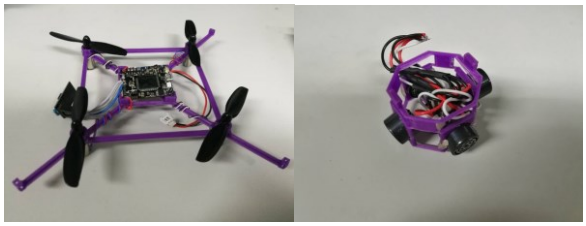

Figure 2. The MAV and sonar platform

The ultrasonic module is installed on the bottom of the MAV, it contains four SFR01 sensors which are perpendicular to each other, and the range measurements of four directions are given separately. The SRF01 sensor is a single transducer ultrasonic sensor, its diameter is 1.6cm and the net weight is about 3g. The maximum measurement distance is 6m and the minimum measurement distance can be reduced to 0cm. The measurement time interval is 200ms.

Fig.3 shows the detection area of the SRF01, it is obtained by placing and measuring the obstacle in the predefined grid points in front of the ultrasonic sensor, and it can be approximated as a polygon.

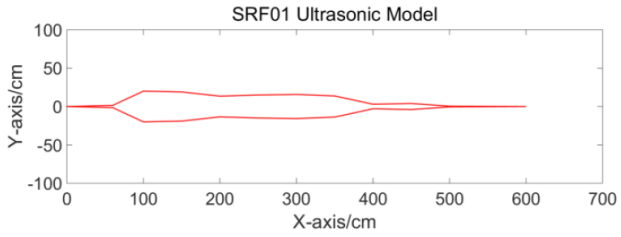

Figure 3. SRF01 polygon model

To reduce the computational load of the polygon model, the multiple-rays model is proposed by connecting the origin to the vertex of the polygon model, as shown in Fig.4.

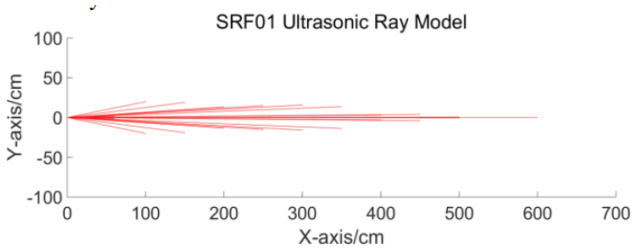

Figure 4. SRF01 multiple-rays model

Thus, the ultrasonic multiple rays model S can be formulated as

$$\begin{cases} \boldsymbol{S}=\{\mathbf{s}_0,\mathbf{s}_1,\mathbf{s}_2,\cdots \\ \boldsymbol{s}_0=\left[x_s,y_s\right]^T \\ \boldsymbol{s}_j=\left[x_s+d_j\cos\theta_j,y_s+d_j\sin\theta_j\right]^T\ (j=1\cdots \end{cases} ,(1)$$

where $\boldsymbol{s}_0=\left[x_s,y_s\right]^T$ denotes the sensor's position in the map coordinate system, d_j and θ_j is the length and the angle of the j^{th} ray, respectively. Then the measurement value is given by

$$\begin{cases} \min\left(\left\|\boldsymbol{q}_1-\boldsymbol{s}_0\right\|_2,\left\|\boldsymbol{q}_2-\boldsymbol{s}_0\right\|_2,\ldots,\ \boldsymbol{q}\quad \boldsymbol{s}_0\right\|_2\right) & \textit{with intersection} \\ q_0 & \textit{without intersection} \end{cases} ,(2)$$

where $\boldsymbol{q}_j=\left[x_j,y_j\right]^T$ is the intersection of the environment and the j^{th} ray, if there is no intersections the measurement value is set to a predefined value q_0. The $\boldsymbol{q}_j$ that minimized (2) is defined as the active intersection, and the i^{th} ray is defined as the active ray of this sonar.

Compared the polygon model, the multiple-rays model may lead to a decrease in the accuracy. When a small obstacle is just in between two adjacent rays, it will not be detected. The resolution of the multiple-rays model is

$$r = \max_{j=1\sim(k-1)} \left(d_j \sin \frac{\theta_{j+1} - \theta_j}{2} \right). \tag{3}$$

The maximum measurement error occurs when the obstacle is just at the polygon boundary, as

$$l_e = \max_{j=1\sim(k-1)} \left(\left| d_{j+1} - d_j \right| \right). \tag{4}$$

For big size obstacle, such as a wall, the multiple-rays model error is related to the angle between the wall and the ultrasonic central axis. Let the angle between the wall and the ultrasonic central axis is φ, the maximum error is

$$l_e = l\left(1 - \sin\left(\varphi + \gamma_j\right)\right), \tag{5}$$

where j represents the j^{th} ray that minimizes (2), i.e., the active ray, and l denotes the true value of the sensor.

III. The Indoor Localization System Modeling

Two coordinate systems, the map coordinate system $O_{m-x_m y_m z_m}$ and body coordinate system $O_{b-x_b y_b z_b}$, are introduced for modeling and navigation of the MAV. O_m is an Earth-fixed and north-east-down(NED) coordinate system where the origin is located at the starting corner m_0 of the map $\boldsymbol{M}$. The matrix $\boldsymbol{M} = [\mathrm{m}_0, \mathrm{m}_2, \ldots$ $R^{2\times(n+1)}$ is the coordinate list of $\mathrm{m}_i = \left[m_{i_x}, m_{i_y} \right]^T \left(i = 0 \sim n \right)$ in counter-clockwise. The origin of the body coordinates is fixed to the center of gravity of the MAV, as shown in Fig.5.

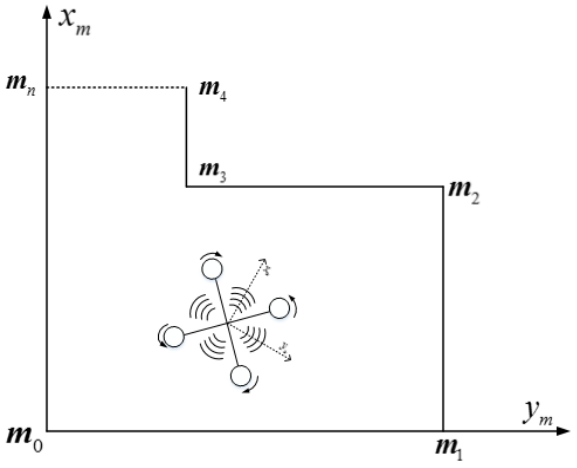

Figure 5. The map coordinate system

Measured by a magnetic sensor, the heading angle of MAV in the map coordinate is given by ψ, thus the rotation matrix from the body coordinate system to the map coordinate system is given by

$$\boldsymbol{R}_{bm} = \begin{bmatrix} \cos\psi & \sin\psi \\ \sin\psi & -\cos\psi \end{bmatrix}, \tag{6}$$

which implies that

$$\boldsymbol{a}_m = \boldsymbol{R}_{bm} \boldsymbol{a}_b, \tag{7}$$

where $\boldsymbol{a}_b$ and $\boldsymbol{a}_m$ denote the acceleration in body coordinate system and in map coordinate system, respectively. Then the discrete state equation of the MAV is given as

$$\boldsymbol{X}(k+1) = \boldsymbol{A} \cdot \boldsymbol{X}(k) + \boldsymbol{B} \cdot \boldsymbol{u}(k), \tag{8}$$

$$\boldsymbol{A} = \begin{bmatrix} 1 & T_A & 0 & 0 \\ 0 & 1 & 0 & 0 \\ 0 & 0 & 1 & T_A \\ 0 & 0 & 0 & 1 \end{bmatrix}, \boldsymbol{B} = \begin{bmatrix} T_A^2/2 & 0 \\ T_A & 0 \\ 0 & T_A^2/2 \\ 0 & T_A \end{bmatrix}, \boldsymbol{u} = \boldsymbol{a}_m(k), \boldsymbol{X} = \begin{bmatrix} x_m \\ v_{m_x} \\ y_m \\ v_{m_y} \end{bmatrix} \tag{9}$$

where $\boldsymbol{X}$ is the state of the MAV, including the position $\left[x_m, y_m \right]$ and the velocity $\left[v_{m_x}, v_{m_y} \right]$ in the map coordinate system, T_A is the sampling period of the accelerometer. The measurement equation is a nonlinear function given by

$$\boldsymbol{l}(k) = \mathrm{h}\left(x_m(k), y_m(k), \psi(k), \boldsymbol{M}, \boldsymbol{S} \right), \tag{10}$$

where $\boldsymbol{l} = \left[l_1 \; l_2 \; l_3 \; l_4 \right]^T$ denotes the distances measured by four sonars.

IV. Indoor Localization Method Based on Extended Kalman Filter

Based on the above MAV model, the EKF algorithm is used to estimate the MAVs location. When both the state equation and the measurement equation are in linear form, the linear KF is an effective approach. However, in this case, the measurement (10) is in a non-linear form, then the EKF can be used. The implementation of EKF and KF are roughly the same, which can be divided into two steps: the prediction and the correction.

The idea of using EKF for state estimation in nonlinear systems is to carry out Taylor expansion of the nonlinear function and omit the second-order and the higher-order terms to obtain the approximate linearized model, and then estimate the system state by the KF. The partial derivative of the measured distance to the system state, which is the Jacobian matrix H of the (10) have a form of (11).

$$\boldsymbol{H} = \frac{\partial \boldsymbol{l}}{\partial \boldsymbol{X}} \tag{11}$$

However, due to the complexity of sonar model and the environment, it is hard to get the explicate form of (10), thus we cannot calculate the Jacobian matrix directly.

In this paper we present a method to calculate the Jacobi matrix. Since the interval between two consecutive sensor samples is small, the following assumptions are made:

- The heading angle of MAV remains unchanged in two adjacent sampling.
- The active ray of the i^{th} sonar remains unchanged in two adjacent sampling.
- The active wall, i.e., the segment of M that has the active intersection with the i^{th} sonar, remains unchanged in two adjacent sampling.

Based on the above assumptions and set a small increment to the MAVs horizontal and vertical position, the specific expression of partial derivative in (11) can be drawn according to the geometric relationship by

$$\begin{cases} \dfrac{\partial l_i}{\partial x_m} = \dfrac{-\sin\alpha_i}{\sin(\alpha_i-\beta_i)}, \dfrac{\partial l_i}{\partial y_m} = \dfrac{\cos\alpha_i}{\sin(\alpha_i-\beta_i)} \\ \dfrac{\partial l_i}{\partial v_{m_x}} = \dfrac{\partial l_i}{\partial v_{m_y}} = 0 \end{cases}, \quad i = 1 \sim 4, \quad (12)$$

where α_i denotes the heading angle of the i th active wall, and β_i denotes the angle between the active ray of the i th sonar and the corresponding active wall.

Note that the accelerometer used in this paper has a sampling period of about 8ms while the ultrasonic sampling period is 200ms, i.e., the accelerometer sampling frequency is much higher than the ultrasound, the strategy is introduced: When the sonar does not get an updated measurement, we use the accelerometer's measurement to calculate the position and variance of the UAV as (13), where Q is the process noise of the system.

$$\begin{cases} \hat{\boldsymbol{X}}(k|k-1) = \boldsymbol{A}\cdot\hat{\boldsymbol{X}}(k-1|k-1) + \boldsymbol{B}\cdot u(k) \\ \boldsymbol{P}(k|k-1) = \boldsymbol{A}\cdot\boldsymbol{P}(k-1|k-1)\cdot\boldsymbol{A}^T + \boldsymbol{Q} \end{cases} \quad (13)$$

And then the result obtained from (13) is directly used as the filtering result of EKF in this step as

$$\begin{cases} \hat{\boldsymbol{X}}(k|k) = \hat{\boldsymbol{X}}(k|k-1) \\ \boldsymbol{P}(k|k) = \boldsymbol{P}(k|k-1) \end{cases}. \quad (14)$$

When the ultrasonic samples new data, it is used to correct the result obtained in (13), the correction step is as (15), where R is the noise variance matrix of the measurement equation.

$$\begin{cases} \hat{\boldsymbol{l}}(k) = h(\hat{x}_m(k|k-1), \hat{y}_m(k|k-1), \psi(k), \boldsymbol{M}, \boldsymbol{S}) \\ \boldsymbol{K}(k) = \boldsymbol{P}(k|k-1)\cdot\boldsymbol{H}(k)^T\cdot\left[\boldsymbol{H}(k)\cdot\boldsymbol{P}(k|k-1)\cdot\boldsymbol{H}(k)^T + \boldsymbol{R}\right]^{-1} \\ \hat{\boldsymbol{X}}(k|k) = \hat{\boldsymbol{X}}(k|k-1) + \boldsymbol{K}(k)\cdot\left[\boldsymbol{l}(k) - \hat{\boldsymbol{l}}(k)\right] \\ \boldsymbol{P}(k|k) = \left[\boldsymbol{I} - \boldsymbol{K}(k)\cdot\boldsymbol{H}(k)\right]\cdot\boldsymbol{P}(k|k-1) \end{cases} \quad (15)$$

The entire EKF algorithm flow is shown as Fig.6.

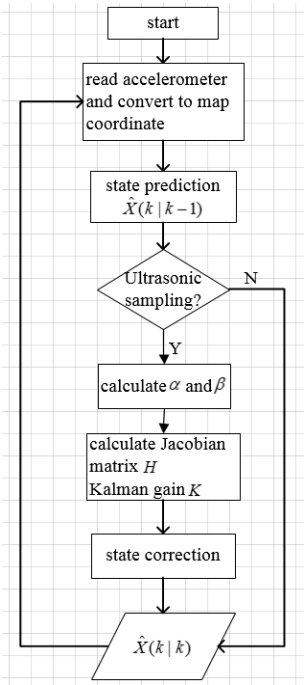

Figure 6. The EKF algorithm flowchart

V. THE SIMULATION RESULTS

The proposed localization algorithm is validated by the simulation in this section. A polygon priori map is given as shown in Fig. (8), and the initial states of the MAV are given by

$$\begin{cases} x_{m0} = y_{m0} = 1(m) \\ v_{mx0} = v_{my0} = 0.05(m/s) \end{cases}$$

The time varying accelerations are used for driving the MAV as Fig.7. According to the MAVs math model, the actual flight path is given in Fig.8

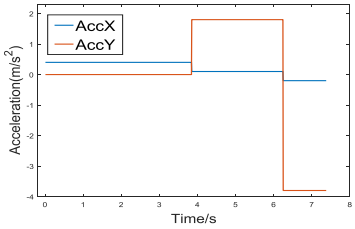

Figure 7. The acceleration data in MAV body axis

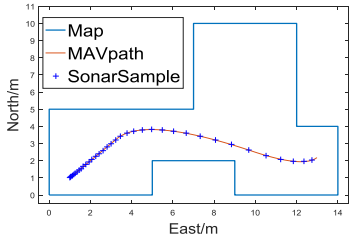

Figure 8. The actual path of the MAV

In Fig.8, the blue line represents the border of the wall, the red line represents MAVs flight path, and "+" corresponds to the MAV position that ultrasonic sensors have a sampling data. The sampled data of accelerometer using in the simulation is formed as

$$a_b = \bar{a}_b + \mathcal{N} \quad , \tag{16}$$

where $\bar{a}_b$ is the true acceleration and $N(0, V_A)$ is a Gaussian noise with variance of V_A.

For a MAV in this map, since the position, the heading angle, the map and the ultrasonic model are known, therefore, the ultrasonic theoretical measurement $\hat{l}$ is known. We also add a Gaussian noise with variance V_S to it, where V_S matches the actual ultrasonic characteristics.

$$l = \bar{l} + \mathcal{N} \tag{17}$$

Table 1 summarizes the parameters used in the simulation.

TABLE I. THE SIMULATION PARAMETERS

Simulation parameter	Value	Units
Accelerometer sample period	8	ms
Sonar sample period	200	ms
Yaw angle	45	°
Accelerometer variance	2.2	m/s^2
Sonar variance	0.007	m
Process noise covariance	$\mathrm{diag}([1, 0.2, 1, 0.2]^T)$	-
Measurement noise covariance	$0.007\mathrm{diag}([1, 1, 1, 1]^T)$	-

In most of the situation, the sonar measurement changes continually over the position of MAV, however in some specific situation it may occurs a jump due to the non-continuity of (10), and this may lead an adverse impact on the localization algorithm. Two typical cases are shown as Fig.9 and Fig.10.

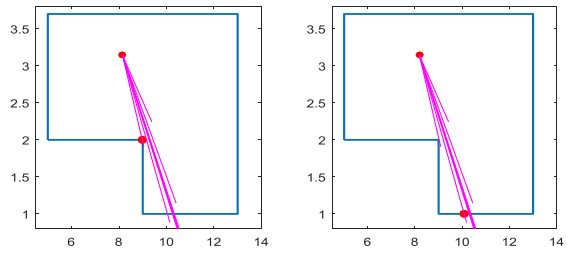

Figure 9. Typical cases 1

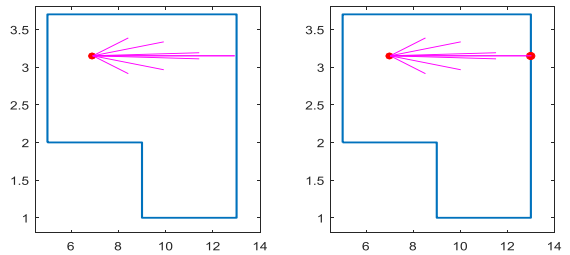

Figure 10. Typical cases 2

As shown in Fig.9, when the MAV is passing a corner, a jump appears in the measurements of the ultrasonic sensor. Fig.10 shows another typical case, when the MAVs distance to the wall is greater than its max measuring range, the ultrasonic will not return a meaningful measurement, as the MAV closes to the wall, the measurement status of ultrasonic will have an abrupt change.

In EKF, these abrupt changes may introduce a jump in the estimation, to solve this problem, a jump filter is given as

$$\begin{cases} K = K(k) \cdot \mathrm{diag}([\lambda_1(k), \lambda_2(k), \lambda_3(k), \lambda_4(k)]^T) \\ \lambda_i(k) = \begin{cases} 1 & \left| \boldsymbol{l}_i(k) - \hat{\boldsymbol{l}}_i(k) \right| \le \varepsilon \\ 0 & \left| \boldsymbol{l}_i(k) - \hat{\boldsymbol{l}}_i(k) \right| > \varepsilon \end{cases}, i \in [1,4] \end{cases} . \tag{18}$$

Therefore, $\boldsymbol{l}(k) - \hat{\boldsymbol{l}}(k)$ term of each ultrasonic is used to filter the jump before the correction step (15). If its value exceeds the predesigned threshold ε, the corresponding measurement will not be used in the estimation.

The localization results of the original EKF and the improved algorithm are shown as Fig.11 and Fig.12.

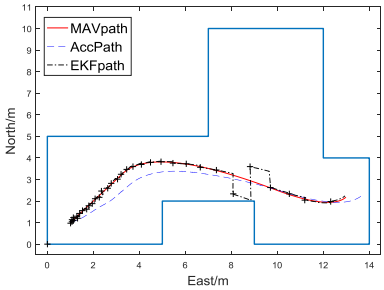

Figure 11. The original EKF localization result

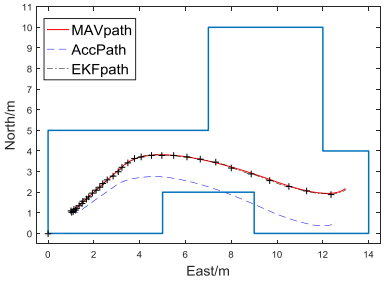

Figure 12. The improved EKF localization result

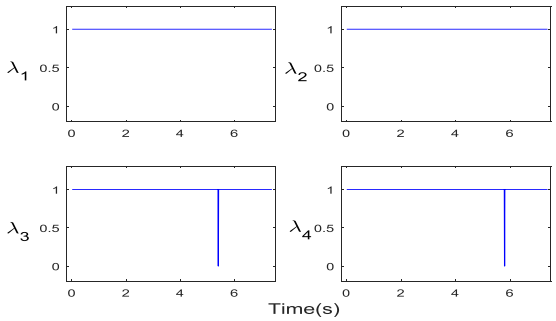

Figure 13. λ_i history during localization

The blue dash line in Fig.11 represents the MAVs position estimated with the integral of accelerometer, it shows the position error is increasing over time due to the drift of the accelerometer, and the localization accuracy is poor. The black line marked with "+" in Fig.11 and Fig.12 show the localization result of the original EKF and our propose approach, respectively. We can see that the original EKF can significantly improve the positioning accuracy in most of the

case, however there are some jumps in the estimation result. As shown in Fig.12, the proposed method is very robust against the abrupt measurement, therefore the positioning accuracy is improved. The curve of λ_i during localization is shown in Fig.13.

The comparison of the estimated position of the original EKF and the improved EKF are shown in Fig.14, where the red line represents localization error of the accelerometer and blue line represents the localization error by proposed algorithm. The simulations results in Table 2 are summarized.

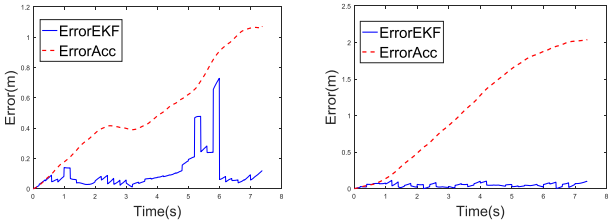

Figure 14. The localization error of original EKF algorithm(lefet) and improved EKF (right)

As shown in Fig.14, compared with the integration of accelerometer, the proposed EKF localization algorithm is more accurate and effective. Table 2 shows that with the addition of the jump filter, the localization error is reduced obviously.

TABLE II. LOCALIZATION ERROR

Localization error	average error(m)	max error(m)
EKF	0.30	2.3
Improved EKF error	0.06	0.58

Considering the low accuracy of the magnetic sensor in practice, the robustness of the localization algorithm against the heading angle is verified. A Gaussian noise with zero mean and 5° covariance is added to the heading angle measurements, and the estimation error is shown in Fig.15.

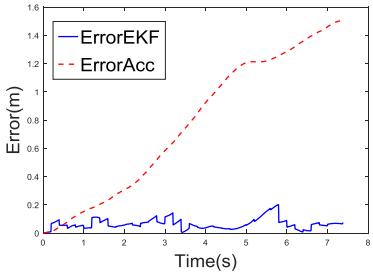

Figure 15. Localization error(with Gaussian noise in yaw angle)

The result shows that the localization errors under the noisy yaw angle remains the same, which reflects the good robustness of the proposed localization algorithm.

VI. CONCLUSION

This paper presents a novel indoor localization algorithm based on EKF, which only relies on four ultrasonic sensors. The computational cost of the algorithm is small and can run in real time on a MAV. Future work is to move the algorithm to the MAV platform to realize the actual operation.

REFERENCES

[1] Chen H, Wang X, Li Y. A Survey of Autonomous Control for UAV[C]// International Conference on Artificial Intelligence and Computational Intelligence. IEEE Computer Society, 2009:267-271.

[2] Grzonka S, Grisetti G, Burgard W. A Fully Autonomous Indoor Quadrotor[J]. IEEE Transactions on Robotics, 2012, 28(1):90-100.

[3] Zheng Z, Liu Y, Zhang X. The more obstacle information sharing, the more effective real-time path planning?[J]. Knowledge-Based Systems, 2016, 114:36-46.

[4] Yassin A, Nasser Y, Awad M, et al. Recent Advances in Indoor Localization: A Survey on Theoretical Approaches and Applications[J]. IEEE Communications Surveys & Tutorials, 2016, PP(99):1-1.

[5] Adewumi O G, Djouani K, Kurien A M. RSSI based indoor and outdoor distance estimation for localization in WSN[C]// IEEE International Conference on Industrial Technology. IEEE, 2013:1534-1539.

[6] Yuan J, Wang X, Dong L, et al. ISILON-An intelligent system for indoor localization and navigation based on RFID and ultrasonic techniques[C]// Intelligent Control and Automation. IEEE, 2010:6625-6630.

[7] Benini A, Mancini A, Longhi S. An IMU/UWB/Vision-based Extended Kalman Filter for Mini-UAV Localization in Indoor Environment using 802.15.4a Wireless Sensor Network[J]. Journal of Intelligent & Robotic Systems, 2013, 70(1-4):461-476.

[8] Elkafrawy K, Youssef M, Elkeyi A, et al. Propagation modeling for accurate indoor WLAN RSS-based localization[J]. 2010:1-5.

[9] Yu L, Fei Q, Geng Q. Combining Zigbee and inertial sensors for quadrotor UAV indoor localization[J]. 2013, 45(5):1912-1916.

[10] Choi J S, Son B R, Kang H K, et al. Indoor localization of Unmanned Aerial Vehicle based on passive UHF RFID systems[C]// International Conference on Ubiquitous Robots and Ambient Intelligence. IEEE, 2013:188-189.

[11] Priyantha N B. The Cricket indoor location system[J]. Massachusetts Institute of Technology, 2005.

[12] Stojkoska B R, Palikrushev J, Trivodaliev K, et al. Indoor localization of unmanned aerial vehicles based on RSSI[C]// IEEE Eurocon 2017 - International Conference on Smart Technologies. IEEE, 2017.

[13] Fan H, Chen Z. WiFi based indoor localization with multiple kernel learning[C]// IEEE International Conference on Communication Software and Networks. IEEE, 2016:474-477.

[14] Li K, Wang C, Huang S, et al. Self-positioning for UAV indoor navigation based on 3D laser scanner, UWB and INS[C]// IEEE International Conference on Information and Automation. IEEE, 2016:498-503.

[15] Shin S, Choi J, Kim B, et al. Improved ultrasonic beacon system for indoor localization[J]. 제어로봇시스템학회 국제학술대회 논문집, 2005.

[16] Opromolla R, Fasano G, Rufino G, et al. LIDAR-inertial integration for UAV localization and mapping in complex environments[C]// International Conference on Unmanned Aircraft Systems. IEEE, 2016:649-656.

[17] Zhao F J, Guo H J, Abe K. A mobile robot localization using ultrasonic sensors in indoor environment[C]// IEEE International Workshop on Robot and Human Communication, 1997. Ro-Man '97. Proceedings. IEEE, 1997:52-57.

[18] Suzuki T, Amano Y, Hashizume T. Vision based localization of a small UAV for generating a large mosaic image[C]// Sice Conference 2010, Proceedings of. IEEE, 2010:2960-2964.

[19] Chenini H, Heller D, Dezan C, et al. Embedded real-time localization of UAV based on an hybrid device[C]// IEEE International Conference on Acoustics, Speech and Signal Processing. IEEE, 2015:1543-1547.

[20] Park S Y, Jung S C, Song Y S, et al. MOBILE ROBOT LOCALIZATION IN INDOOR ENVIRONMENT USING SCALE-INVARIANT VISUAL LANDMARKS[J]. 2010.

[21] Liu T, Zhang W, Gu J, et al. A Laser Radar based mobile robot localization method[J].

[22] Khoshelham K. Automated localization of a laser scanner in indoor environments using planar objects[C]// International Conference on Indoor Positioning and Indoor Navigation. IEEE, 2010:1-7.